Chalcogenide Letters Vol. 22, No. 8, August 2025, p. 735 - 752

The impact of laser energy of pure CdS and CdS: Cu nano structured thin films on their structural, morphological, and optical properties as gas sensors

A. W. Jabbar [a], N. K. Abbas [b*]
[a] *Department of Physics Laser Institute for Postgraduate Studies, University of Baghdad, Iraq*
[b] *Department of Physics, College of Science for Women, University of Baghdad, Baghdad, Iraq*

Nanostructured CdS and CdS: Cu thin films were synthesized by pulsed laser deposition with a Nd: YAG laser of different energies, 0.1, 0.5, and 1 W. The number of pulses was 300, and the frequency was 20 kHz. The CdS nanoparticles were deposited on a glass substrate. The optical, structural, and morphological properties were investigated utilized X-ray diffraction, UV-Vis spectrophotometry, and field emission scanning electron microscopy. From 2.25 to 2.1 eV, the results demonstrate that the band gap energy reduces as laser energy increases. Morphological investigations reveal that the laser energy has a significant impact on the nanoparticles' size. The average diameter of the produced nanoparticles increases from 45 to 56 nm with increasing energy. A gas sensor for gas (NO2) was created, and the impact of increasing temperature on gas sensitivity, Response time, and Recovery time was investigated.

(Received May 15, 2025; Accepted August 18, 2025)

Keywords: CdS:Cu semiconductors, structural, and morphological, Nanostructure, Laser, CdS nanofilms

1. Introduction

The direct band gap of cadmium sulfide (CdS), a dimeric semiconductor, is 2.42 eV at ambient temperature. The properties of its thin films depend on several factors, including the deposition method and rate, the type and temperature of substrate, temperature, and the pressure. CdS is can be used in various optoelectronic applications, such as photoluminescence, electroluminescence, photoconductivity, and photovoltaic devices [1–2]. Numerous deposition methods, including chemical bath deposition (CBD) [3–4], electrodeposition [5], chemical spray pyrolysis (CSP) [6], spin coating [7], vacuum evaporation [8], screen printing [9], flash evaporation [10], sputtering [11], molecular beam epitaxy (MBE) [12], and pulsed laser deposition (PLD) [13–14], can be used to produce CdS thin films. These methods can produce films with different crystalline structures, grain sizes, and optical and electrical properties. The most important characteristics of PLD technology compared to other physical and chemical deposition methods [15] are: (a) it is simple and straightforward; (b) Various gases and pressures can be used to deposit different materials.; (c) it is inexpensive; and (d) by controlling the pulsed laser parameters, the film growth characteristics can be controlled. (e) It is scalable, as PLD can achieve the desired film stoichiometry for multi-element materials compared to other deposition techniques, and thin films of various materials with strong adhesion, such as insulators, metals, and semiconductors, can be created. This technology is scalable, achieving the required bonding ratio for films of multi-component materials compared to other deposition techniques. Additionally, it makes it possible to produce thin films with strong adhesion from a variety of materials. PLD has recently become an important technology for producing high-quality semiconductor films [16]. Several studies have thoroughly examined cadmium sulfide (CdS) thin films because of their wide range of applications [17–19]. In this work, pure cadmium sulfide and

* Corresponding author: nadaka_phys@csw.uobaghdad.edu.iq
https://doi.org/10.15251/CL.2025.228.735

copper-doped cadmium thin films were fabricated using PLD technology due to their aforementioned advantages.The evaporation source was a Nd:YAG laser operating at 1064 nm. The prepared samples were characterized structurally, morphologically, and optically. In order to assess the synthetic material's potential for gas sensing applications, several laser intensities were used to examine their impact on the material's particle size.

2. Experimental procedure

2.1. Materials

Every chemical used in this project came from Sigma-Aldrich, including cadmium acetate ($Cd(CH_3COO)_22H_2O$), thiourea (CH_4N_2S), copper, the hydraulic piston from laryee technology company (china), Nd:YAG laser from Wuxi Raycus Fiber Laser Technologies CO, glass substrate and all of the experiments were conducted with deionized.

2.2. Characterization

A Siemens D500 system (CuK=0.154 nm) was used to record X-ray diffraction (XRD) patterns of pure CdS and CdS:Cu. Field-emission scanning electron microscopy (FESEM) was performed using a ZEISS/SigmaVP model at a magnification of 50.00 KX/Oxford. Reflectance spectroscopy (Shimadzu) was used in the wavelength range (300-800 nm) for analysis.

2.3. Cadmium sulfide nanoparticle preparation

A 0.1 M solution of cadmium acetate ($Cd(CH_3COO)2.2H_2O$) was made. Sodium hydroxide (NaOH), a soluble ionic compound that contains the hydroxide ion (OH^-), was gradually added to the solution after it had been placed on a magnetic stirrer until the pH value dropped between 8 and 9. To fully combine the ingredients, 0.1 M thiourea (CH_4N_2S), a sulfur source, is then added and magnetically stirred for two hours. After that, the manufactured material is allowed to dry and powder for a whole day.

2.4. Synthesis of CdS:Cu

The nano-CdS material impregnated with Cu is prepared in the following proportions 3, 4, and 5 wt% for 1 h after preparing the pure CdS material. The Cu material is added in different weights and according to the percentage of CdS. It is then placed on a magnetic stirrer for another 4 h until it turns brown.

2.5. Preparation of thin film

In this work, hydraulic pistons were used to make targets from CdS powder. CdS and CdS: Cu targets were prepared in pellet form, 3 mm in thickness, 10 mm in diameter, by grinding the material into a homogeneous fine powder using 1.5 g of material and pressing with 8 tons of pressure for 10 min. In addition, PLD was used to make CdS thin films, which were produced using different laser energies, 1, 0.5, and 0.1 W, at a pressure of P=3.5×10-5 mbar for 200 pulses per energy. The PLD source was a Nd: YAG laser operating at a fundamental wavelength of 1064 nm and a frequency of 6 Hz. The laser was aimed at the target at a 45° angle, and the material was deposited on the substrate 3 cm away from the target.

3. Results and discussion

3.1. Characterization of structure

The X-ray diffraction patterns of pure CdS films produced with varying laser energy are displayed in Fig. 1. The graphic shows that all of the samples contain polycrystalline cubic and hexagonal structures, which is consistent with the standard card number 96-900-8863. As the laser energy increases, the position of the tip will have some deviations due to the different lattice voltages as the crystal size changes [20].

Additionally, it can be observed that, as laser energy increases, the peak's intensity grows a nd its width decreases, suggesting that crystallinity is rising and crystal size is still increasing. The crystal size increases with the increase of laser energy, allowing the removal of a larger mass of target material, and higher energy also causes small particles to fuse [21]. Table 1 shows the most characteristic structures.

Table 1. XRD data of pure CdS nanocrystalline thin film with power 1, 0.5, and 0.1 W

	2Ɵ(Deg)	**FWHM(Deg)**	**dhkl (Å)**	**C.s(nm)**	**Phase**	**hkl**
0.1	26.565	0.734	3.3528	11.1	Cub. CdS	(111)
	30.289	0.262	2.9485	31.4	Cub. CdS	(200)
	36.451	0.472	2.4629	17.7	Hex. CdS	(102)
	43.846	0.682	2.0631	12.6	Cub. CdS	(220)
	52.080	0.996	1.7547	8.9	Cub. CdS	(311)
0.5	26.565	0.551	3.3528	14.8	Cub. CdS	(111)
	30.236	0.341	2.9535	24.1	Cub. CdS	(200)
	36.451	0.262	2.4629	31.9	Hex. CdS	(102)
	43.794	0.787	2.0655	10.9	Cub. CdS	(220)
	51.844	0.839	1.7621	10.5	Cub. CdS	(311)
1	24.939	0.656	3.5676	12.4	Hex. CdS	(100)
	26.539	0.577	3.3560	24.1	Cub. CdS	(111)
	28.112	0.734	3.1717	21.2	Hex. CdS	(101)
	36.504	0.551	2.4595	35.2	Hex. CdS	(102)
	43.925	0.787	2.0596	10.9	Cub. CdS	(220)
	47.675	0.734	1.9060	21.8	Hex. CdS	(103)
	52.054	0.787	1.7555	11.2	Cub. CdS	(311)

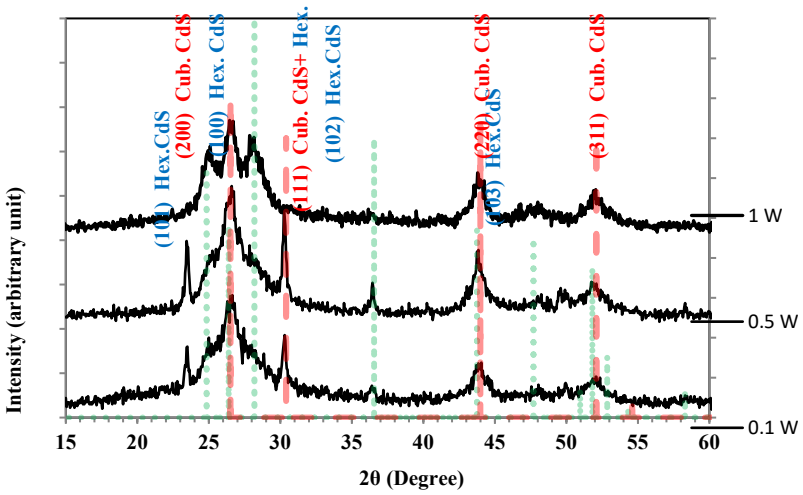

Fig. 1 XRD Pattern of pure CdS thin films with different energies.

The impact of laser energy on the structural characteristics of nanocrystalline CdS is displayed in Figs. 2, 3, and 4. Cu thin films. The standard card number 96-900-886 is compatible with the polycrystalline, hexagonal, and cubic structures found in all spectra, according to XRD data. It can be concluded that CdS: Cu has a hexagonal structure, and the diffraction peaks are located at (111) and (200) of the crystal, corresponding to 43.2 ° and 50 °, respectively. Additionally, the findings demonstrate that as the laser energy rises from 0.1 to 1 W, the intensity increases continuously, and the grain size also increases. As the copper content in the crystal increases, the crystal's size has shrunk, as seen by the diffraction peaks becoming increasingly scattered. [22-23]. It was observed that the low-quality samples have a hexagonal phase, while the high-quality samples have a cubic phase [24-25]. Tables (2) to (4) show the most characteristic structures

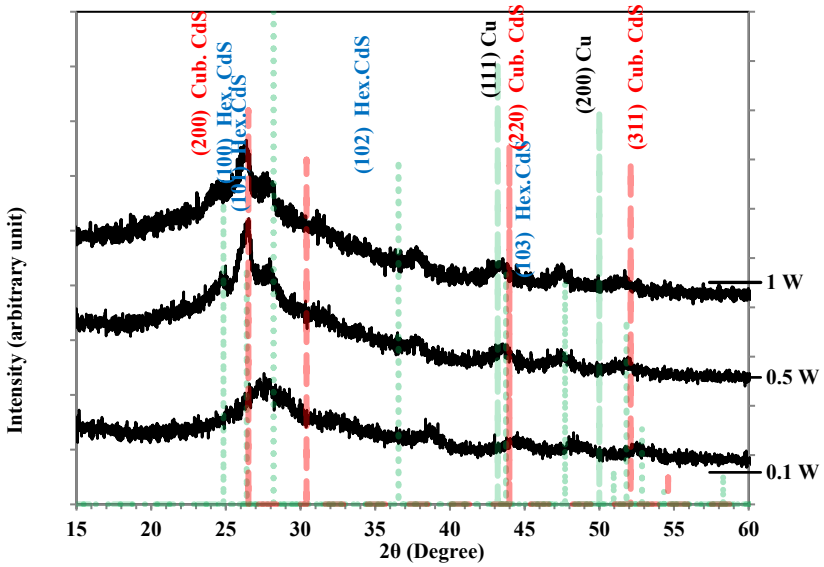

Fig. 2. XRD pattern of CdS:Cu (3%) nanocrystalline thin films with varied laser energies.

Table 2. XRD data of CdS:Cu (3%) thin nanocrystalline film with power 1, 0.5 and 0.1W.

Power (w)	2Θ(Deg)	FWHM (Deg)	dhkl (Å)	C.s(nm)	Phase	hkl
0.1	24.969	0.893	3.5634	9.1	Hex. CdS	(100)
	26.614	0.988	3.3466	8.3	Cub. CdS	(111)
	28.119	0.846	3.1709	9.7	Hex. CdS	(101)
	43.683	1.035	2.0705	8.3	Cub. CdS	(220)
	47.680	1.035	1.9058	8.4	Hex. CdS	(103)
	51.959	1.129	1.7585	7.8	Cub. CdS	(311)
0.5	24.969	0.376	3.5634	21.6	Hex. CdS	(100)
	26.614	0.423	3.3466	19.3	Cub. CdS	(111)
	28.354	0.423	3.1451	19.4	Hex. CdS	(101)
	43.872	0.470	2.0620	18.2	Cub. CdS	(220)
	48.151	0.564	1.8883	15.4	Hex. CdS	(103)
1	25.016	0.470	3.5568	17.3	Hex. CdS	(100)
	26.661	0.705	3.3408	11.6	Cub. CdS	(111)
	28.401	0.470	3.1400	17.4	Hex. CdS	(101)

Table 3. XRD data of CdS:Cu (4%) nanocrystalline thin film with power 1, 0.5 and 0.1 W.

Power (w)	2Θ(Deg)	FWHM (Deg)	dhkl (Å)	C.s(nm)	Phase	hkl
0.1	24.969	0.893	3.5634	9.1	Hex. CdS	(100)
	26.614	0.988	3.3466	8.3	Cub. CdS	(111)
	28.119	0.846	3.1709	9.7	Hex. CdS	(101)
	43.683	1.035	2.0705	8.3	Cub. CdS	(220)
	47.680	1.035	1.9058	8.4	Hex. CdS	(103)
	51.959	1.129	1.7585	7.8	Cub. CdS	(311)
0.5	24.969	0.376	3.5634	21.6	Hex. CdS	(100)
	26.614	0.423	3.3466	19.3	Cub. CdS	(111)
	28.354	0.423	3.1451	19.4	Hex. CdS	(101)
	43.872	0.470	2.0620	18.2	Cub. CdS	(220)
	48.151	0.564	1.8883	15.4	Hex. CdS	(103)
1	25.016	0.470	3.5568	17.3	Hex. CdS	(100)
	26.661	0.705	3.3408	11.6	Cub. CdS	(111)
	28.401	0.470	3.1400	17.4	Hex. CdS	(101)
	36.724	0.611	2.4452	13.7	Hex. CdS	(102)
	43.872	0.423	2.0620	20.2	Cub. CdS	(220)
	48.103	0.846	1.8900	10.3	Hex. CdS	(103)

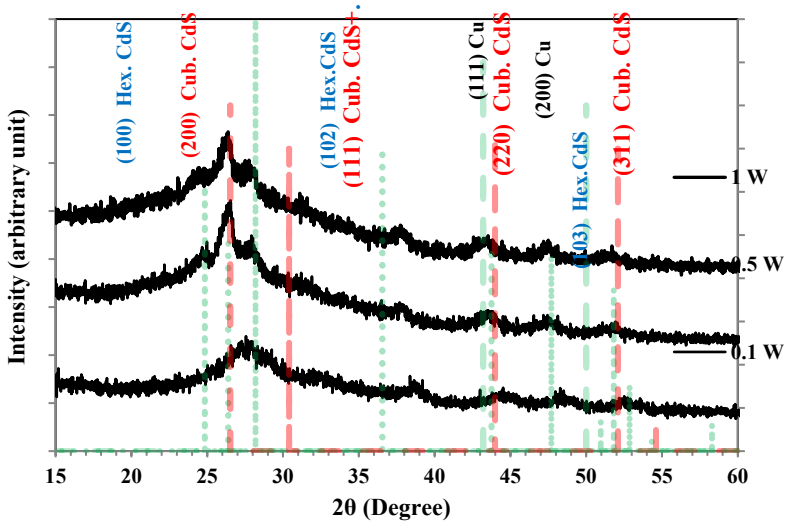

Fig. 3. XRD pattern of CdS:Cu(4%) nanocrystalline thin films with different laser energies.

Table 4. XRD data of CdS:Cu (5%) nanocrystalline thin film with power 1, 0.5 and 0.1 W.

Power (w)	2Θ(Deg)	FWHM (Deg)	dhkl (Å)	C.s(nm)	Phase	hkl
0.1	25.767	2.188	3.4547	3.7	Cub. CdS	(111)
0.5	24.781	0.772	3.5900	10.5	Hex. CdS	(100)
	26.454	0.944	3.3666	8.6	Cub. CdS	(111)
	27.998	1.073	3.1843	7.6	Hex. CdS	(101)
	43.613	0.815	2.0736	10.5	Cub. CdS	(220)
	47.388	0.858	1.9169	10.1	Hex. CdS	(103)
1	24.824	0.686	3.5838	11.9	Hex. CdS	(100)
	28.084	0.729	3.1748	11.2	Hex. CdS	(101)
	43.613	0.901	2.0736	9.5	Cub. CdS	(220)
	47.688	0.815	1.9055	10.7	Hex. CdS	(103)
	51.935	0.944	1.7592	9.4	Cub. CdS	(311)

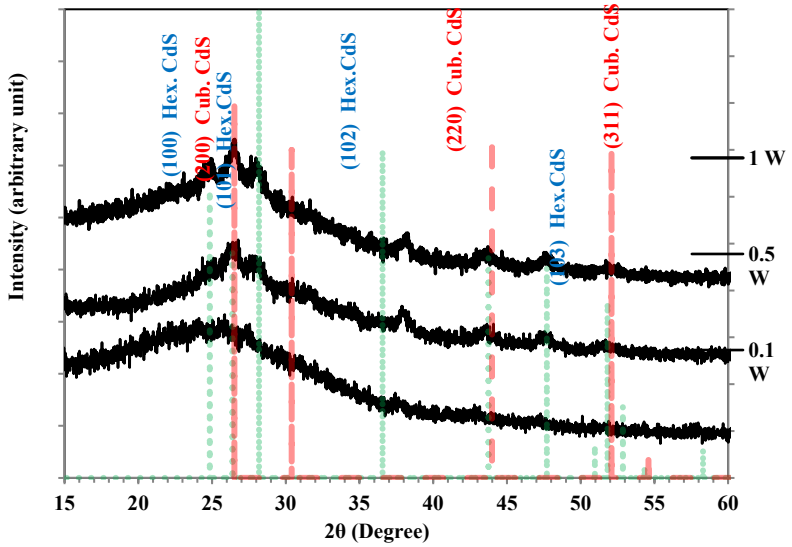

Fig. 4. XRD pattern of CdS:Cu (5%) nanocrystalline thin films with different laser energies.

3.2. The field emission scanning electron microscope (FE-SEM)

Images from SEM of pure CdS nanocrystalline thin film at different laser energies are shown in Fig. 5. The micrographs show that the microstructures of these composites are very similar except for a slight increase in particle aggregation.

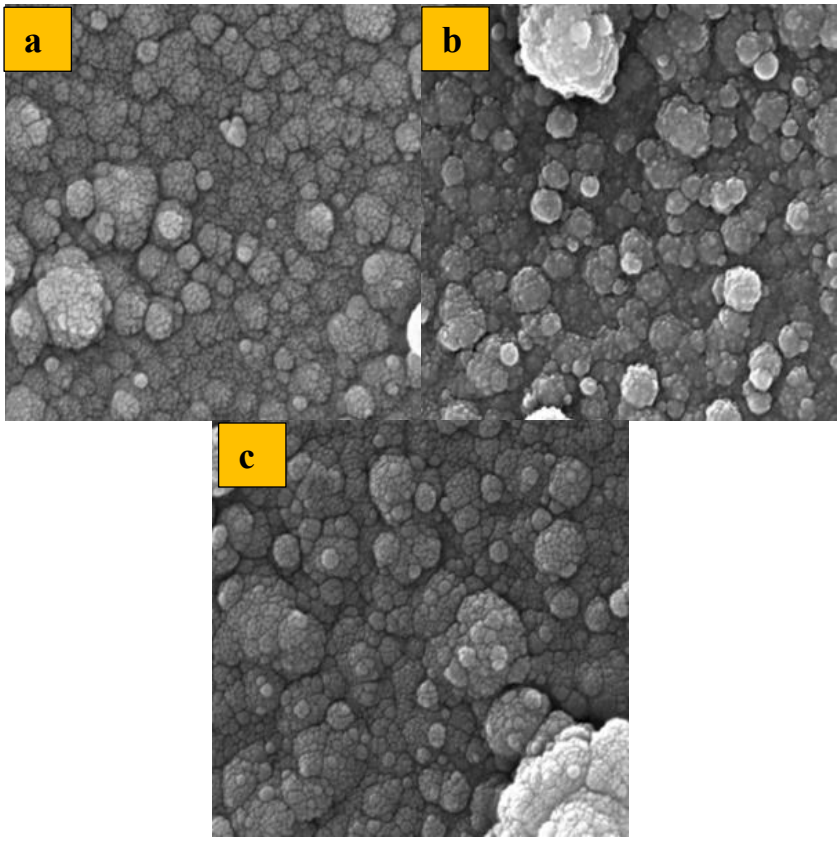

Fig. 5. FESEM for pure CdS nanocrystalline thin film with different energies PLD (a, b and c are 0.1, 0.5 and 1 w respectively)

The Entropy may increase with increasing growth temperature (laser power). This results in reduced binding between OH- ions and nanocrystals in the matrix solution, and more nanocrystals can interact with each other, leading to increased particle aggregation at higher laser power. The morphological characteristics of pure copper and 3, 4, and 5 weight percent Cu-doped nanocrystalline films produced at various laser strengths are displayed in Figs. 6–8. The surface of the substrate is heavily coated with particles in every sample, and these particles are dispersed nearly evenly across the surface. The 5% Cu-doped film has larger grains than the 3 and 4% Cu-doped films, which have smaller grains. The CdS film is essentially (purely) permeable. The pores are nearly round and dispersed irregularly. The arrows indicate that the pores have random forms or blend into lines. When Cu is added, the porosity of the CdS film reduces. Then, it decreases when the copper ratio increases to 4%; it increases when the copper concentration increases to 5%. For the 3% and 5% Cu-doped films [26].

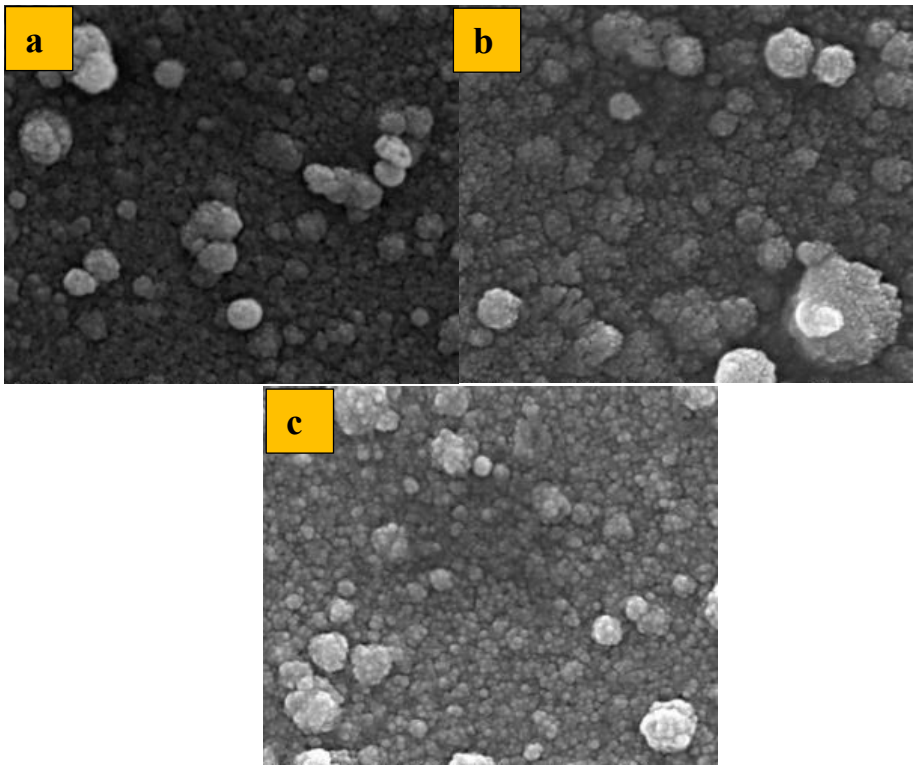

Fig. 6. FESEM for CdS:3% at wt Cu for the nanocrystalline thin film with different energies (PLD: a, b, and c are 0.1, 0.5, and 1 W respectively).

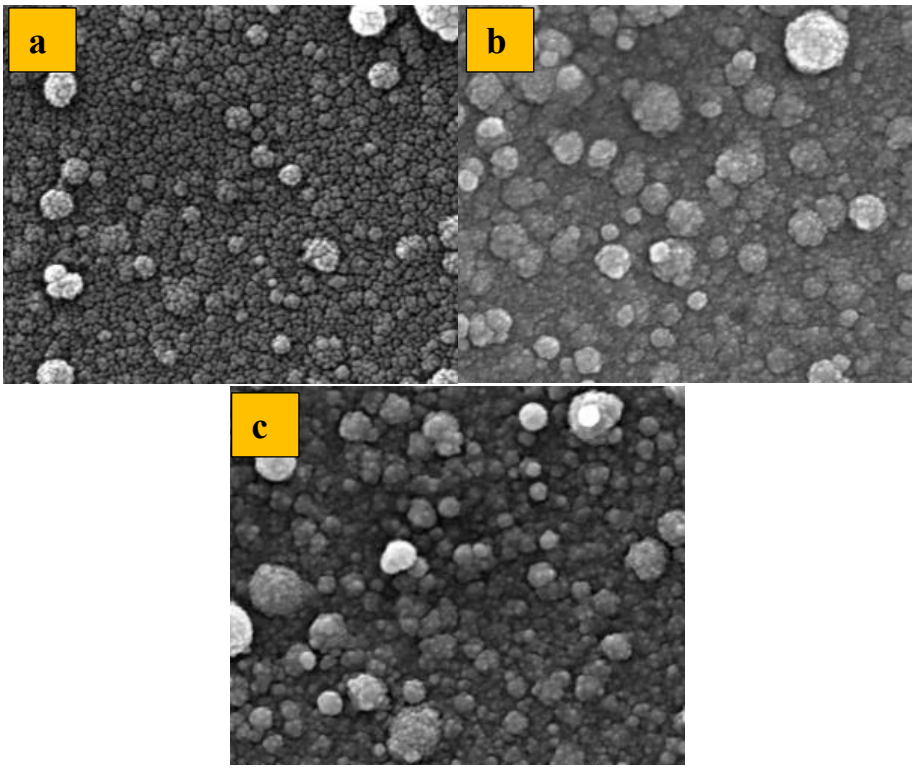

Fig. 7. FESEM for CdS:4% at wt CU for the nanocrystalline thin film with different energies (PLD: a, b, and c are 0.1, 0.5, and 1 W respectively).

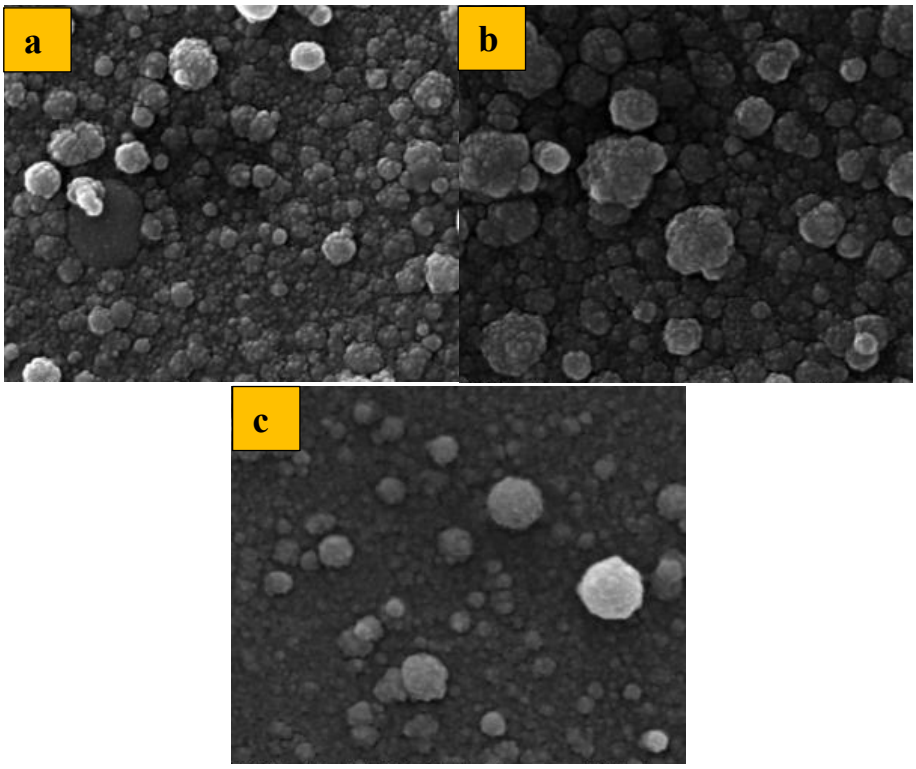

Fig. 8. FESEM for CdS:5% at wt CU for the nanocrystalline thin film with different energies (PLD: a, b, and c are 0.1, 0.5, and 1 W respectively).

3.3. Optical characterization

The widening energy gap plays a crucial role in deciding the applications of the films prepared, including detectors and solar cells. Figure 9 illustrates the energy gap values of pure CdS and doped with 3%, 4%, and 5% wt of Cu films fabricated at varying laser intensities. The rising deposition energy results in a significant reduction in the values of the prohibited energy gap, calculated using the following equation. 1 [27].

$$\alpha h\upsilon = A\,(h\upsilon - Eg)^{r} \quad (1)$$

where hυ represents the photon energy, Eg is the energy gap, r is the type of transition, and A is a constant. The direct transition is permitted when the values are 1/2 and 3/2, the indirect transition is permitted when the values are 2 and 3, and the direct transition is prohibited when the values are 3/2.

The reduction in the energy gap can be explained by the fact that raising the laser power causes a noticeable rise in the quantity of photon collisions with the material, which in turn causes the material to absorb more photons. As a result, there are more electrons and vacancies, which eventually causes the energy gap to decrease. There are a number of reasons why the energy gap value has decreased, including the organization of the atomic distribution within the material, changes in crystalline phases, and the type of material, which is achieved by changing the deposition energy [29]. A change in the lattice constant or an increase in crystal size could potentially be the cause of this decline. [27]. In addition, it is attributed to grain agglomeration [28]. Fig. 10 shows that as the laser power increases, more photons are absorbed because the energy gap decreases and new localized states appear within the band gap. Ahmed et al. [30] reached the same result.

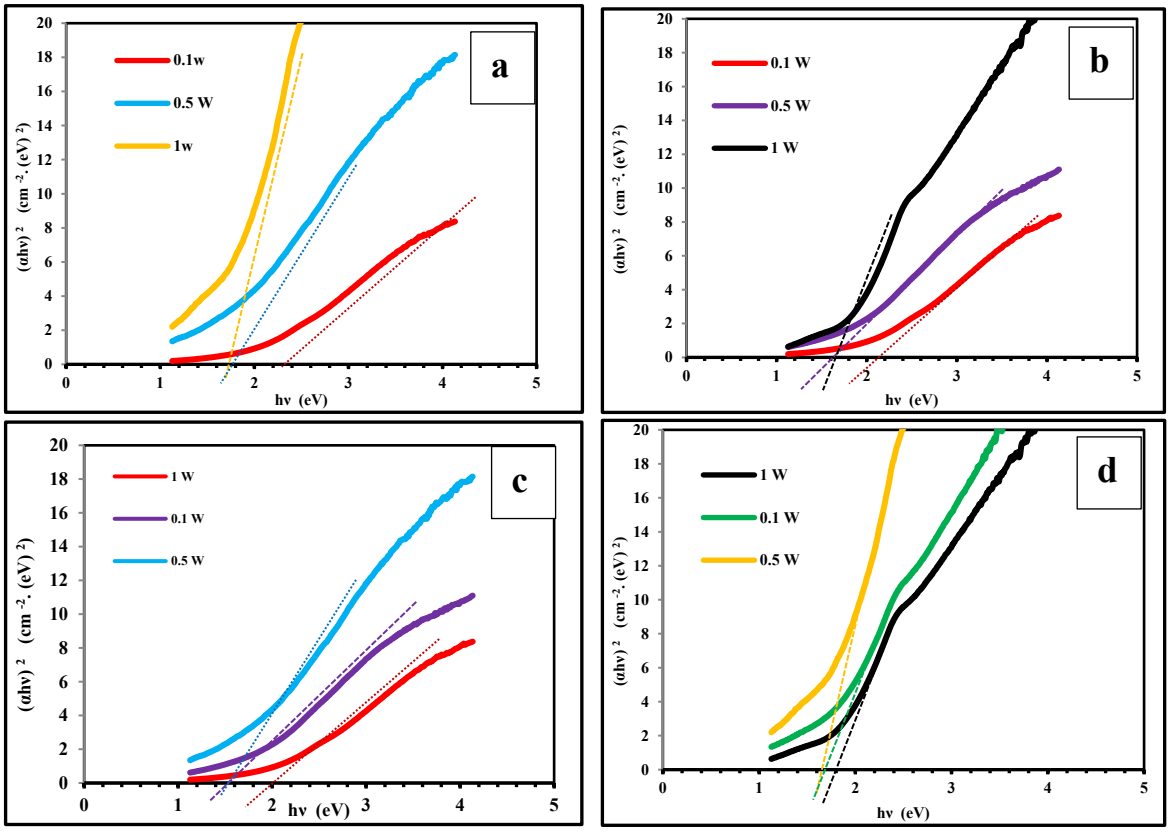

Fig. 9. Direct transition of pure CdS(a), (b) CdS:Cu 3%, (c) CdS:Cu 4% and (d) CdS:Cu 5% prepared by PLD at different laser energies.

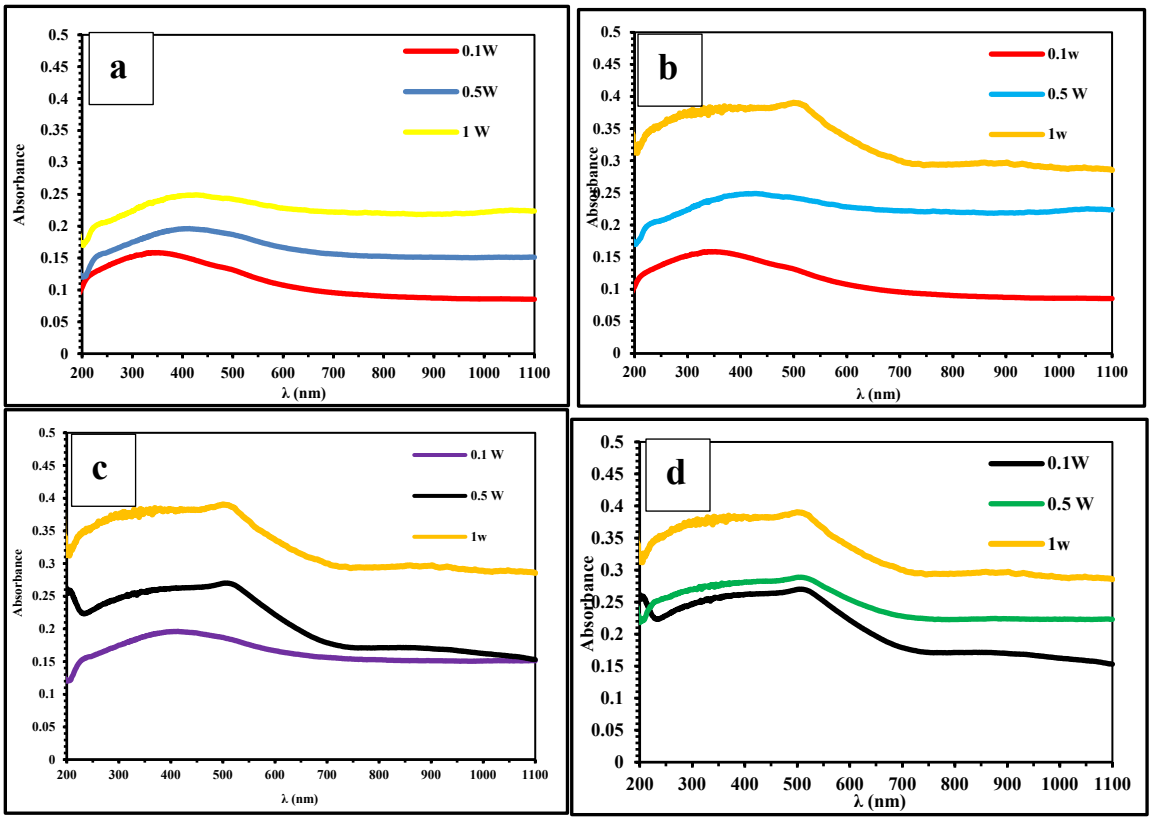

Fig. 10. Absorbance spectrum of (a) pure CdS (b) CdS:Cu 3% (c) CdS:Cu 4% and (d) CdS:Cu 5% films prepared by PLD at different laser energy.

3.4. Gas sensor measurements

This study evaluated the gas-detecting capabilities of NO_2 sensors at various temperatures.

The percentage of sensitivity to NO2 was calculated from equations (S (%) = x100% for n-type for oxide gas [31]); Fig. 11 shows the change of sensitivity values of pure CdS films with changing temperature for different laser powers. Table 5 shows the change of sensitivity values, response and recovery time with changing temperature for different laser powers.

It is crucial to identify gas sensors and emphasize the operating temperature. The efficacy of the fabricated sensors, consisting of pure CdS and CdS: Cu (3% and 5%), has been evaluated at operational temperatures between 30 °C and 200 °C.

As the operating temperature increases for pure CdS, the responses of all sensors accelerate rapidly. At a predetermined temperature, the reactions reached their maximum intensity. The sensitivity increases to its maximum value of 43.33 at 200°C. The sensitivity also rises as the laser energy decreases. The decrease in laser energy leads to diminished nanoparticle dimensions, hence improving the adsorption of gas molecules onto the nanomaterial. Increased laser intensity yields larger crystal sizes, facilitating the collection of more target material and promoting the aggregation of smaller particles [32,33]. Small granular particles expand the acceptable boundaries for interactions between gas and oxygen. This combination will expedite the process, hence enhancing sensitivity [34]. For pure CdS with varying laser energy, Fig. 12 displays the response time as a function of temperature. We can observe that the reaction time lowers as laser energies decrease because of the reduction in particle size. Fig. 13 shows how the healing time changes with temperature for CdS when using different laser powers. Fig. 14 shows the change of sensitivity values of CdS:3%Cu films with changing temperature for different laser powers. The reaction time is less than the recovery time, as shown by the two graphs. This indicates the successful creation of a high-quality sensor. CdS: Cu 5% responds to NO2 gas at a temperature of 30°C as a result of its decoration, which causes an increase in the active sites for absorbing gas molecules, as shown in Fig. (17). The sensing response reached 41.1 in comparison with the pure

CdS and the CdS: Cu3% NPs samples. This improvement in the sensing response is due to the increase in the adsorption kinetics of gaseous atoms on the surface of CdS: Cu 5%. Figures (15and 18) displays the reaction time in relation to temperature for CdS: Cu 3% and CdS:Cu 5% respectively, while figures (16 and 19) show the recovery time according to temperature for CdS: Cu 3% and CdS: Cu 5% respectively. Figures show that the response time is shorter than the recovery time, which indicates that a suitable sensor is obtained. All samples exhibited the highest sensitivity to NO2 gas at 200°C.

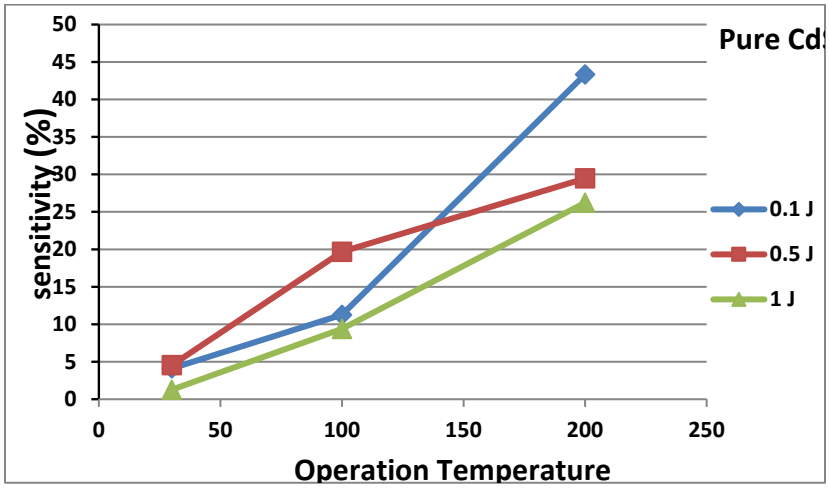

Fig. 11. Represents the relationship between sensitivity and operating temperature for pure CdS films at different laser powers.

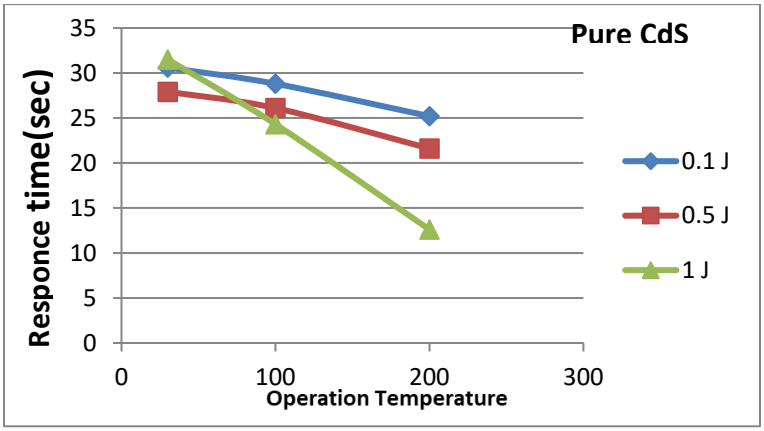

Fig. 12. Represents the relationship between response time and operating temperature for pure CdS films with different laser powers.

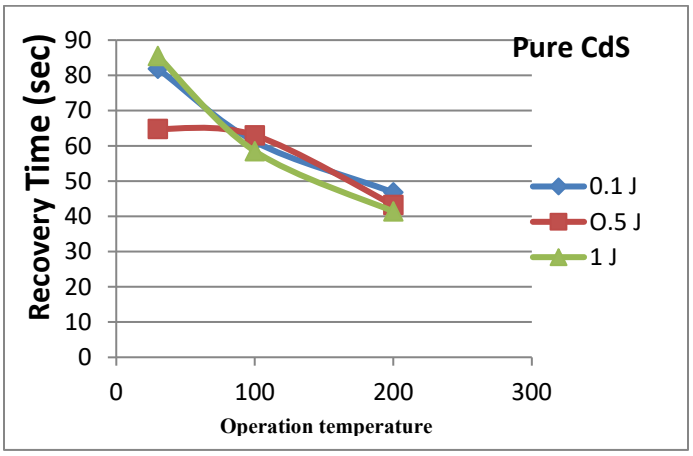

Fig. 13. Represents the relationship between recovery time and operating temperature for pure CdS films with different laser powers.

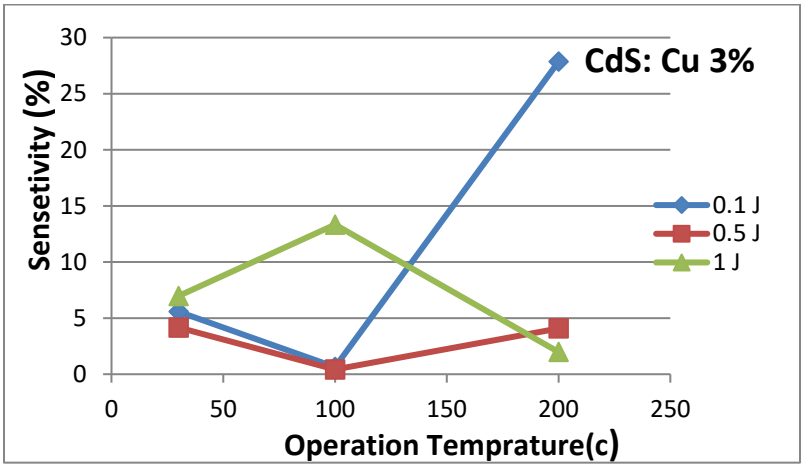

Fig. 14. Represents the relationship between sensitivity and operating temperature for CdS: Cu 3% films at different laser powers.

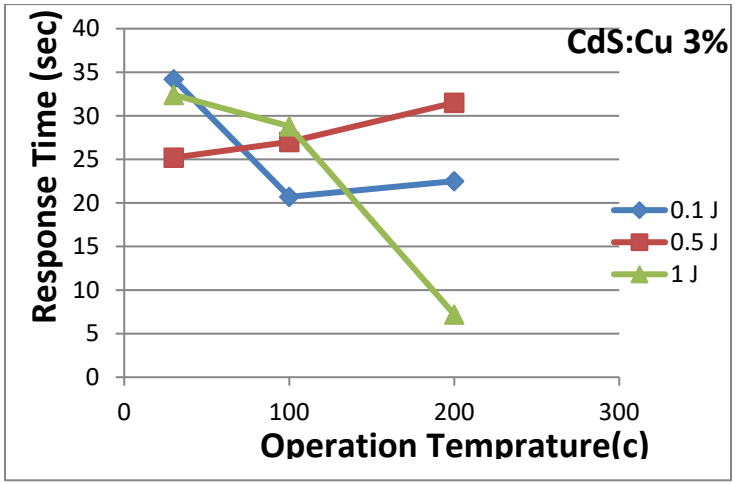

Fig. 15. Represents the relationship between response time and operating temperature for CdS: Cu 3% films with different laser powers.

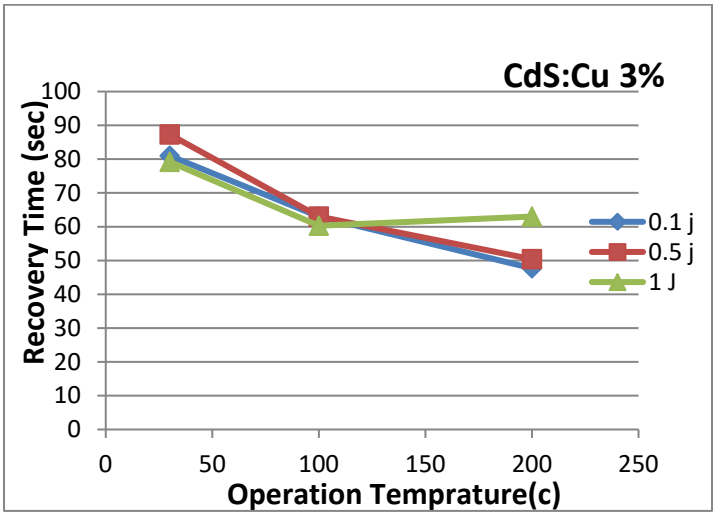

Fig. 16. Represents the relationship between recovery time and operating temperature for CdS: Cu 3% films with different laser powers.

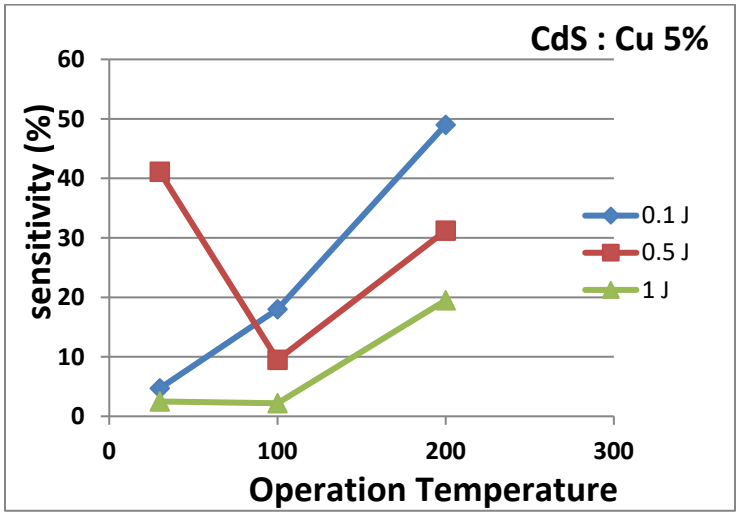

Fig. 17. Represents the relationship between sensitivity and operating temperature for CdS: Cu 5% films at different laser power.

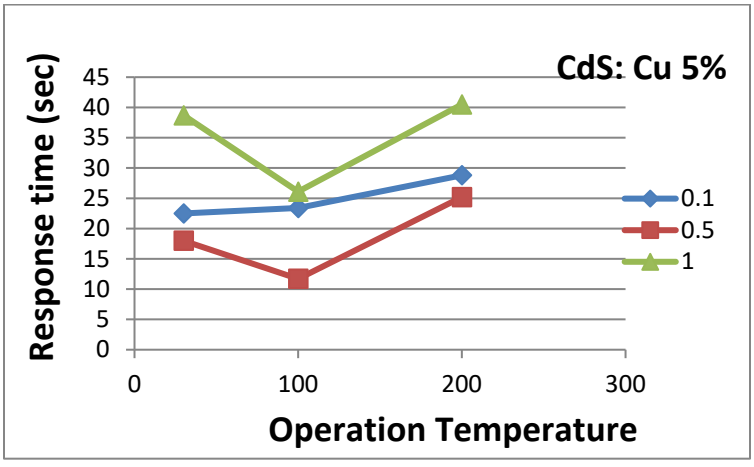

Fig. 18. Represents the relationship between response time and operating temperature for CdS: Cu 5% films with different laser powers.

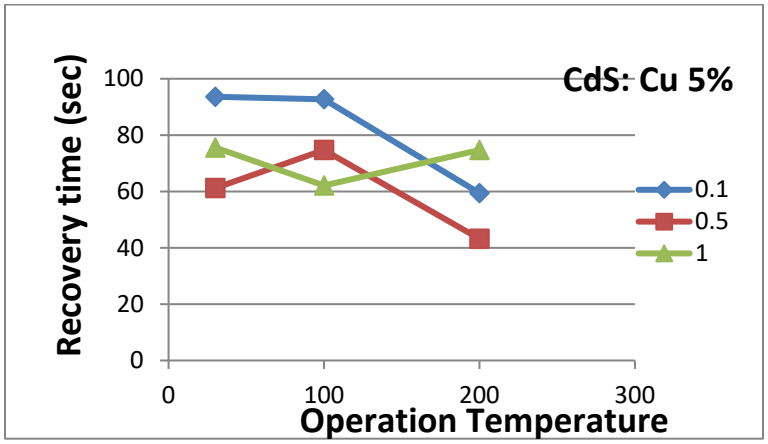

Fig. 19. Represents the relationship between recovery time and operating temperature for CdS: Cu 5% films with different laser powers.

Table 5. Values of sensitivity percentage, response and recovery time for NO_2 gas and corresponding operating temperatures for different laser powers.

concentration	0.1 W				0.5 W				1 W			
	Temp(ºC)	Sensitivity %	Res Tim (sec)	Rec Tim(sec)	Temp(ºC)	Sensitivity%	Res Tim (sec)	Rec Tim(sec)	Temp(ºC)	Sensitivity%	Res Tim (sec)	Rec Tim(sec)
Pure CdS	30	4.12	30.6	81.9	30	4.54	21.6	64.8	30	1.26	31.5	85.5
	100	11.26	28.8	61.2	100	19.6	26.1	63	100	9.38	24.3	58.5
	200	43.33	25.2	46.8	200	29.4	27.9	27.9	200	26.2	21.6	41.4
CdS:Cu 3%	30	5.58	34.2	81	30	4.16	25.2	87.3	30	6.97	32.4	79.2
	100	0.64	20.7	63	100	0.42	27	63	100	13.3	28.8	60.3
	200	27.86	22.5	47.7	200	4.08	31.5	50.4	200	1.98	7.2	63
CdS:Cu 5%	30	4.79	22.5	93.6	30	41.1	18	61.2	30	2.55	38.7	75.6
	100	18	23.4	92.7	100	9.5	11.7	74.7	100	2.24	26.1	62.1
	200	48.67	28.8	59.4	200	31.2	25.2	43.2	200	19.9	40.5	74.7

4. Conclusion

Using pulsed laser deposition, copper thin films containing cadmium sulfide and cadmium sulfate were effectively created on glass substrates. The films were made at room temperature in a vacuum. X-ray diffraction (XRD), optical absorption spectroscopy, and field-emission electron microscopy (FESEM) were used to examine the films, and optical absorption spectroscopy. The peak height increases with increasing laser power, while their width decreases, indicating improved crystallinity. Elevating the energy of the laser pulse causes the lattice constant or crystal size to shift, increasing the absorbance of all deposited films while decreasing the energy gap for all samples, both of which are important parameters in sensors. Based on the sensitivity and response time results, it is possible to use the cadmium sulfide and cadmium sulfate: copper nanostructured films to obtain a good gas sensor.

References

[1] J. Nanda, S. Sapra, D. D. Sarma, Size-Selected Zinc Sulfide Nanocrystallites: Synthesis, Structure, and Optical Studies, Chem. Mater. 12(4), 1018 (2000); https://doi.org/10.1021/cm990583f

[2] T. J. Hussien,K.A. Nada ,A.A.Al-Attraqchi, Azhar ,International Journal of Drug Delivery Technology, 10 (3),378-382 2020). https://impactfactor.org/PDF/IJDDT/10/IJDDT,Vol10,Issue3,Article13.pdf

[3] K. C. Wilson, M. B. Ahamed, Appl. Surf. Sci., 361, 277-282 (2016); https://doi.org/10.1016/j.apsusc.2015.11.184

[4] I. Perlikowski, E. Zielony, T. Özdal, H. Kavak, Energies, 14(16), 5182 (2021); https://doi.org/10.3390/en14165182

[5] Y. Zhang, H. Ma, D. Wu, R. Li, X. Wang, Y. Wang, W. Zhu, Q. Wei, B. Du, Biosens Bioelectron, 77, 936-936 (2016); https://doi.org/10.1016/j.bios.2015.10.074

[6] S.Yılmaz, Y. Atasoy, M. Tomakin, E. Bacaksız, Superlattices Microstruct. 88, 299-307 (2015); https://doi.org/10.1016/j.spmi.2015.09.021

[7] W. Kim, M. Baek, K. Yong, Sens. Actuators B Chem., 223, 599-605 (2016); https://doi.org/10.1016/j.snb.2015.09.158

[8] T. Özdal, T. Chtouki, H. Kavak, V. Figa, D. Guichaoua, H. Erguig, J. Mysliwiec & B. Sahraoui, J. Inorg. Organomet. Polym. Mater., 31, 89-99 (2021); https://doi.org/10.1007/s10904-020-01646-y

[9] J. Trajic, M. Gilic, N. Romcevic, M. Romcevic, G. Stanisic, B. Hadzic, M. Petrovic, Y. Yahia, Sci. Sinter., 47(2), 145-152 (2015); https://doi.org/10.2298/SOS1502145T

[10] N. Croitoru, S. Jakobson, Thin Solid Films, 56(3), L5-L7 (1979); https://doi.org/10.1016/0040-6090(79)90144-5

[11] V. Canevari, N. Romeo, G. Sberveglieri, S. Azzi, A. Tosi, M. Curti, L. Zanotti, J. Vac. Sci. Technol. A, 2, 9-10 (1984); https://doi.org/10.1116/1.572636

[12] A. Piel, H. Murray, Thin Solid Films, 44(1), 65-73 (1977); https://doi.org/10.1016/0040-6090(77)90028-1

[13] K. A. Aadim, N. K. Abbas, and A. T. Dahham ,Baghdad Science Journal , 15(3), 292-298(2018); http://dx.doi.org/10.21123/bsj.2018.15.3.0292

[14] Y. Bleu, F. Bourquard, T. Tite, A. Loir, C. Maddi, C. Donnet, F. Garrelie, Front. Chem., 6, 572 (2018); https://doi.org/10.3389/fchem.2018.00572

[15] Z. O. Elhmaidi, M. A.-Lefdil, M. A. El Khakani, Nanomaterials, 10(7), 1393 (2020); https://doi.org/10.3390/nano10071393

[16] M. Jelínek, V. Trtík, L. Jastrabík, Pulsed laser deposition of thin films, Physics and Materials Science of High Temperature Superconductors, IV, 215-231 (1997); https://doi.org/10.1007/978-94-011-5732-2_16

[17] S. N. Ogugua, O. M. Ntwaeaborwa, H. C. Swart, Coatings, 10(11), 1078 (2020); https://doi.org/10.3390/coatings10111078

[18] V. H. Martínez-Landeros, N. Hernandez-Como, G. Gutierrez-Heredia, M. A. Quevedo-Lopez, F. S. Aguirre-Tostado, Thin Solid Films, 682, 24-28 (2019); https://doi.org/10.1016/j.tsf.2019.05.014

19. J.A. Abd, W.M. Mohammed, A. Al-Nafiey, Key Eng. Mater., 882, 155-164 (2021); https://doi.org/10.4028/www.scientific.net/KEM.882.155

20. W. S. Hussein, A. F. Ahmed, K. A. Aadim, Iraqi J. Sci., 61(6), 1307-1312 (2020); https://doi.org/10.24996/ijs.2020.61.6.8

[21] D. Bhattacharya, Pramana J. Phys., 55, 823-833 (2000); https://doi.org/10.1007/s12043-000-0050-0

[22] J. Fred O'Shay, Time-Resolved Visible and Extreme Ultraviolet Spectroscopy of Laser-Produced Tin Plasma, Ph.D Dissertation, University of California, San Diego USA, (2007).

[23] J. Yang, R. Liu, S. Huang, Y. Shao, Y. Huang, Y. Yu, Catal. Today, 224, 104-113 (2014); https://doi.org/10.1039/c3ra42445f

[24] P. Roy, S. K. Srivastava, J. of Physics D: Appl. Phys., 39(22), (2006); https://doi.org/10.1088/0022-3727/39/22/006

[25] S. Kose, F. Atay, V. Bilgin, I. Akyuz, E. Ketenci, Appl. Surf. Sci., 256(13), 4299-4303 (2010); https://doi.org/10.1016/j.apsusc.2010.02.018

[26] S. J. Lade, M. D. Uplane, C. D. Lokhande, Mater. Chem. Phys., 53(3), 239-242(1998); https://doi.org/10.1016/S0254-0584(97)02071-3

[27] N. K. Abbas, Z. J. Shanan, T. H. Mohammed, Baghdad Science Journal, 19(1), 217-224 (2022); https://doi.org/10.21123/bsj.2022.19.1.0217

[28] M. Shaban, M. Mustafa, A. M. El Sayed, Materials Science in Semiconductor Processing, 56, 329-343(2016); https://doi.org/10.1016/j.mssp.2016.09.006

[29] V. K. Unnikrishnan, K. Alti, V. B. Kartha, C. Santhosh, G. P. Gupta, B. M. Suri, Pramana J. Phys., 74(6), 983-993, (2010); https://doi.org/10.1007/s12043-010-0089-5

[30] R.H. Ahmed, A.M.E. Ibrahim, K.A. Aadem, Tikrit Journal of Pure Science, 23(10), 72-75. (2019); https://doi.org/10.25130/tjps.v23i10.566

[31] J.R.Aseel, 2021, Modify the Surface of ZnO Nanorod Arrays using Organic (Eosin-Y) Dye for Gas Sensor .M.sc. Iraq: University of Baghdad/ master thesis.

[32] L. Chopra, S.R. Das, Thin film solar cells, Springer Science & Business Media, 304, 1983; https://doi.org/10.1007/978-1-4899-0418-8

[33] N.K.Abbas, A.F. Abdulameer, R.M. Ali, S.M. Alwash, Silicon, 2019, 11(2), pp. 843-855; https://doi.org/10.1007/s12633-018-9874-4

[34] S.I. Hasan,A. Naje, Q.G.Al-zaidi, 2014, International Journal of Current Engineering and Technology, 4(6), PP.3954-3960.(2014).